Efficiency Optimization of a DSP-Based Standalone PV System Using Fuzzy Logic and Dual-MPPT Control

Ahmad Al Nabulsi and Rached Dhaouadi, *Senior Member, IEEE*

***Abstract*—This paper presents a new digital control scheme for a standalone photovoltaic (PV) system using fuzzy-logic and a dual maximum power point tracking (MPPT) controller. The first MPPT controller is an astronomical two-axis sun tracker, which is designed to track the sun over both the azimuth and elevation angles and obtain maximum solar radiation at all times. The second MPPT algorithm controls the power converter between the PV panel and the load and implements a new fuzzy-logic (FLC)-based perturb and observe (P&O) scheme to keep the system power operating point at its maximum. The FLC-MPPT is based on a voltage control approach of the power converter with a discrete PI controller to adapt the duty cycle. The input reference voltage is adaptively perturbed with variable steps until the maximum power is reached. The proposed control scheme achieves stable operation in the entire region of the PV panel and eliminates therefore the resulting oscillations around the maximum power operating point. A 150-Watt prototype system is used with two TMS320F28335 eZdsp boards to validate the proposed control scheme performance.**

***Index Terms*—Digital signal processor, fuzzy logic controller (FLC), maximum power point tracking (MPPT), physical tracking, standalone photovoltaic (PV) system.**

I. Introduction

SIGNIFICANT progress has been made over the last few years in the research and development of renewable energy systems such as wind, sea wave and solar energy systems. Among these resources, solar energy is considered nowadays as one of the most reliable, daily available, and environment friendly renewable energy source [1], [2].

However, solar energy systems generally suffer from their low efficiencies and high costs [3]. In order to overcome these drawbacks, maximum power should be extracted from these systems using either physical tracking or maximum power point tracking (MPPT). Physical tracking involves aligning the photovoltaic (PV) panels to be orthogonal to the sun rays throughout the day in order to receive maximum solar radiation [4]–[11].

This tracking can be done manually or automatically. In manual tracking, the PV panel orientation is manually changed at the beginning of each season to a predetermined angle. In the case of automatic tracking, the PV panel is mounted on a single-axis or multi-axis tracking mechanism and is controlled to follow the sun rays trajectory throughout the day [4]–[11]. The tracking mechanisms can be classified into three types, namely, passive method, optical method, and the astronomical method. The general features that characterize an efficient tracking mechanism are: ability to cover a wide range of space, robustness against wind disturbances, and low-power consumption.

Passive tracking is based on the heating properties of gas matters such as Freon [5]. The tracker is composed of two cylindrical tubes fitted on the edges of the panel; these tubes are filled with a fluid under partial pressure. Sun heat will increase the sun side cylinder gas pressure causing an unbalance in the tracker. As a result, the tracker will tilt to the sun side. This type of system is relatively cheap and needs little maintenance. However, it has lower efficiency compared to other types of trackers, especially at low temperatures, moreover they have not yet been widely accepted by consumers [4].

The second method of tracking is the optical or electro-optic trackers. This method uses feedback sensors such as photo-sensors, current, voltage sensors, and auxiliary cells to determine the panel reference position [6]–[8]. A closed-loop position control system based on fuzzy logic or PID is used to produce the actuators control commands. The drawback for such a system is that it is very sensitive to atmospheric conditions (clouds shading) and might not be able to continue tracking the sun in a cloudy day.

The third tracking method is the astronomical method, which employs the longitude and latitude data of a given location to determine the sun current position [9]–[11]. The main advantage of this method over the optical method is that it involves simpler programming, reduced implementation cost, and lower power consumption as the need for additional sensors is eliminated. This method also provides high degree of accuracy and is not sensitive to atmospheric conditions.

In addition to physical tracking, MPPT can be used to optimize the efficiency of PV systems. MPPT is a real-time control scheme applied to the PV system charger in order to extract the maximum power possible from the PV panel.

The MPPT working principle is based on the maximum power transfer theory. The power delivered from the source to the load is maximized when the input resistance seen by the source matches the source resistance. Therefore, in order to transfer maximum power from the panel to the load the internal resistance of the panel has to equal the resistance seen by the PV panel. For a fixed load, the resistance seen by the panel can

Manuscript received November 28, 2011; revised February 25, 2012; accepted March 06, 2012. Date of publication April 03, 2012; date of current version July 23, 2012. Paper no. TII-11-811.

The authors are with the American University of Sharjah, 26666, Sharjah, UAE (e-mail: rdhaouadi@aus.edu).

Color versions of one or more of the figures in this paper are available online at http://ieeexplore.ieee.org.

Digital Object Identifier 10.1109/TII.2012.2192282

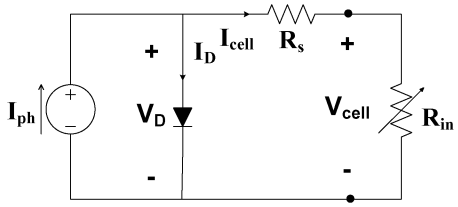

Fig. 1. PV system circuit model.

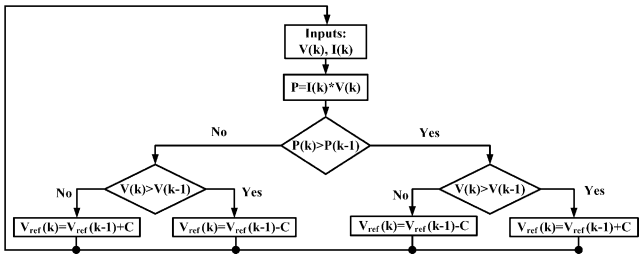

Fig. 2. P&O algorithm operation.

be adjusted by changing the charger (DC/DC converter) duty cycle [12]–[14]. Fig. 1 further illustrates the PV system input resistance concept.

The literature is rich with various MPPT techniques varying in implementation complexity, cost, adjustability to different PV systems, and overall produced efficiency [15]–[41].

The Hill Climbing (HC) and the Perturb and Observe (P&O) are the most known and commercially used techniques [19]–[27]. Other methods such as the incremental Conductance (INC) technique [28]–[31], the neural network (NN) technique [32]–[34] and fuzzy logic controller technique [35]–[38] have been also widely reported. The working principle of the HC-MPPT technique is summarized as follows. The PV panel voltage and current are measured at fixed sampling intervals and fed to the controller to calculate the PV panel power. The power increment $\Delta P(k) = P(k) - P(k-1)$ is calculated at each sampling time and according to its sign, the duty cycle is incremented or decremented in fixed steps depending on the voltage values until the maximum power point (MPP) is reached.

The P&O technique shares the same HC concept of operation, but with an additional PI control loop [22]. In the P&O, the converter, input reference voltage is the perturbed variable and the duty cycle is computed through the additional PI control loop. The additional control loop results in an increase in the P&O efficiency, as the system demonstrates a faster dynamic performance and better regulated PV output voltage compared to HC [22]. The operation of the P&O technique is explained by the flowchart given in Fig. 2.

As seen from the flow chart, the system operating point will stay oscillating around the MPP. The size of the oscillation will depend on the chosen perturbation step C. In general, the smaller the step the lesser the oscillations, but that will be on the expense of the system convergence speed to the MPP. Hence, in spite of their popularity and ease of implementation, these two techniques suffer from a low overall efficiency resulting from the oscillations. In order to overcome these drawbacks the use of modified adaptive techniques and the introduction of three-point weight comparison P&O algorithm are suggested.

In the three-point weight comparison method [23], [24], the duty cycle is perturbed in both sides of the operating point and then the power slope at the current operating point is compared to the power slope at the two perturbed points. If the sign of the slope is changed between the two perturbed points, then the current operating point is the MPP and the perturbation stops. Although this technique results in less oscillation, it requires an additional point reading resulting in more computations and a slower system.

In the modified adaptive techniques, the step size C of the P&O/HC is modified based on the operating point location [25]–[27]. The system starts with a large step size but starts decreasing it until the operating point reaches the MPP. The main disadvantage of this technique is determining the suitable factor by which the step size has to be modified as it depends on the PV system configuration.

Recently, high-performance Digital Signal Processors (DSP)-based platforms have been introduced in many real-time control applications [42], [43]. These platforms offer great flexibility for real-time testing and validation of different control schemes, rapid prototyping, and a significant reduction in implementation work [44], [45].

This paper proposes a new DSP controlled dual-MPPT scheme based on fuzzy logic control (FLC). The first MPPT controller is an astronomical two-axis sun tracker that keeps maximum radiation on the panel throughout the day. The second controller implements a new fuzzy-based MPPT technique to adaptively change the P&O perturbation step size depending on the PV system operating point and the current step size. The proposed control scheme achieves stable operation in the entire region of the PV panel and eliminates therefore the resulting oscillations around the maximum power operating point. The small signal analysis model of the power converter is presented along with a Lyapunov-based stability analysis of the PV system.

II. PV System Description

The proposed standalone photovoltaic system consists of four main blocks: PV panel, solar tracker, DC/DC converter (charger), and the MPPT controller. The following sections will describe the modeling of each component.

A. PV Panel Model

The PV panel model used in our analysis is the single-diode model [39]–[41]. This model represents the illuminated solar cell in its simplest form as a PN junction, as shown in Fig. 1

$$V_{\text{cell}} = V_D - I_{\text{cell}} R_s \tag{1}$$

$$I_{\text{cell}} = I_{ph} - I_D = I_{ph} - I_o \left(e^{K_{PV}(V_{pv} + I_{pv} R_s)} - 1 \right) \tag{2}$$

where V_{cell} and I_{cell} are the PV cell terminal voltage and current, V_D and I_D are the diode voltage and current, $K_{PV} = q/pKT$ with the electron charge $q = 1.6 \times 10^{-19} C$, K is the Boltzmann's constant, T is the cell temperature, and $p = 1.3$ is the ideal p-n junction characteristic factor for monocrystalline solar cells. I_{ph} is the photocurrent given by

$$I_{ph} = (I_{sc} + K_I(T - T_r)) \frac{\lambda}{100} \tag{3}$$

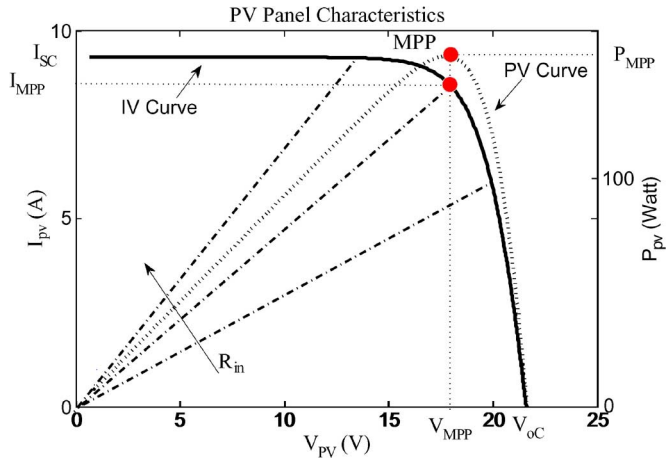

Fig. 3. PV panel characteristics.

TABLE I
PV PANEL PARAMETERS

P_{max}	V_{max}	I_{max}	V_{OC}	I_{SC}	N_p	N_s
50 W	17.3 V	8.7 A	21.6 V	9.3 A	2	36

where I_{sc} is the short-circuit cell current at reference temperature and insolation, K_I (mA/K) is the short-circuit current temperature coefficient, λ is the insolation in (MW/cm^2), and I_o is the saturation current in diode reverse-biased direction

$$I_o = I_{rr}\left(\frac{T}{T_r}\right)^3 e^{\left(\frac{qV_g\left(\frac{1}{T_r}-\frac{1}{T}\right)}{pK}\right)} \tag{4}$$

where I_{rr} is the reverse saturation current at the reference temperature T_r, V_g is the band gap voltage of the semiconductor making up the cell, which equals 1.12 eV for xtal Si cells

$$R_s = -\frac{dV}{dI_{V_{oc}}} - \frac{1}{X_V} \tag{5}$$

$$X_V = I_o \times \frac{q}{pKT}\left(e^{\frac{qV_{oc}}{pKT}}\right). \tag{6}$$

The PV panel model can be computed using (2) by taking into consideration the number of cells connected in series N_s and in parallel N_p as follows:

$$I_{\text{panel}} = N_p I_{ph} - N_p I_o\left(e^{\left(\frac{K_{pv}(V_{pv}+I_{pv}R_s)}{N_s}\right)} - 1\right). \tag{7}$$

The PV panel power is computed by multiplying (7) with the PV voltage V_{panel}

$$P_{\text{panel}} = N_p I_{ph} V_{pv} - N_p I_o V_{pv}\left(e^{\left(\frac{K_{pv}(V_{pv}+I_{pv}R_s)}{N_s}\right)} - 1\right). \tag{8}$$

The panel IV and PV characteristics curves are obtained by plotting the PV current and PV power as a function of the PV voltage, as shown in Fig. 3. Table I shows the parameters of the PV panel used. Fig. 3 illustrates also the location of three important points on the PV panel characteristics; the short-circuit current (I_{sc}), the open-circuit voltage (V_{oc}), and the maximum power point $(P_{\text{MPP}}, I_{\text{MPP}}, V_{\text{MPP}})$.

Fig. 4. Front view of the solar tracker mechanism (panel in vertical position).

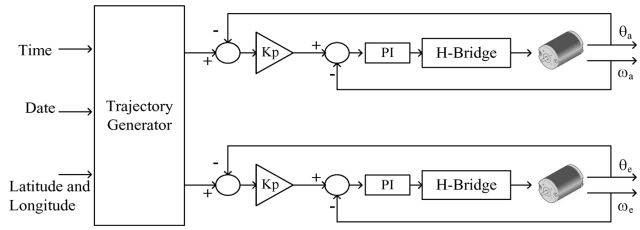

Fig. 5. Block diagram of the control system.

B. Solar Tracker

In order to track the sun trajectory, a two-axis tracker with a 150-Watt PV panel was manufactured, as illustrated in Fig. 4 [11]. The tracker base has a rotary table mechanism with a DC motor and a worm gear drive that rotates the panel about the vertical axis. The rotary table includes in addition a thrust bearing that is able to support the load caused by the weight of the structure. The panel is held using a frame, which is mounted on top of the rotary table.

The panel is tilted around the horizontal axis using another DC motor connected to the panel through a gear with a ratio 240:1. The tracker is controlled using an astronomical angular trajectory generation. Given the date, time, latitude, and longitude of the current location of the system, the DSP controller calculates the sun reference azimuth and elevation angles using preimplemented equations. The panel azimuth and elevation angles are next controlled to follow their reference values using digital closed loop position control, as shown in Fig. 5. Incremental optical encoders are connected to the motor shafts to provide the angular position and speed information to the DSP to implement the control algorithm.

C. Power Converter Model

The developed standalone PV system uses a buck converter as a power processing unit. The buck converter circuit consists of a MOSFET switch and a diode, in addition to a filter circuit based on a capacitor and an inductor as shown in Fig. 6. The circuit is controlled through a PWM signal generated by the MPPT controller.

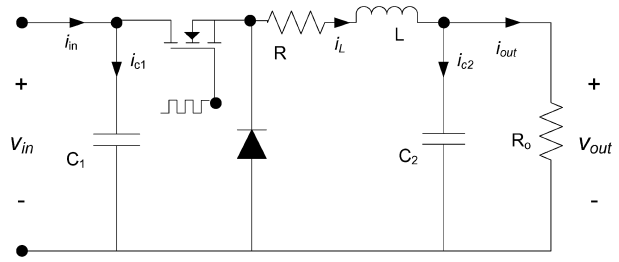

Fig. 6. Buck converter circuit.

To design the MPPT control system, it is necessary to model the converter dynamic behavior. In particular, it is of interest to determine how variations in the input current $i_{\rm in}(t)$, the load current $i_{\rm out}(t)$ and the duty cycle $d(t)$ affect the input voltage $v_{\rm in}(t)$.

The state-space averaging technique is used next to generate the low-frequency small-signal ac equations of the PWM DC-DC converter [46].

The buck converter is assumed to operate in a continuous conduction mode with two states based on the status of the power switch. In the first state $0 \le t \le t_{\rm on}$, the switch is ON. Applying Kirchoff's laws on the converter circuit yields

$$v_{\rm in} = v_L + v_{\rm out} = i_L R + L\frac{di_L}{dt} + v_{\rm out} \tag{9}$$

$$i_{\rm out} = i_L - i_{C2} = i_L - C_2\frac{dv_{\rm out}}{dt} \tag{10}$$

$$i_L = i_{\rm in} - i_{C1} = i_{\rm in} - C_1\frac{dv_{\rm in}}{dt}. \tag{11}$$

Taking the inductor current i_L, output voltage $v_{\rm out}$, and input voltage $v_{\rm in}$ as state variables, these equations can be written in the following state-space form

$$\begin{cases} \dot{X} = A_1 X + B_1 u \\ y = E_1 X + F_1 u \end{cases} \tag{12}$$

where $u = i_{\rm in}$, $y = v_{\rm in}$, and $X = [i_L\ v_{\rm out}\ v_{\rm in}]^t$.

In the second state $t_{on} \le t \le T$, the switch will be OFF. Analyzing this circuit yields

$$i_{\rm in} = i_{C1} = C_1\frac{dv_{\rm in}}{dt} \tag{13}$$

$$i_{\rm out} = i_L - i_{C2} = i_L - C_2\frac{dv_{\rm out}}{dt} \tag{14}$$

$$v_L = i_L R + L\frac{di_L}{dt} = -v_{\rm out}. \tag{15}$$

The equations can be also written in state-space form

$$\begin{cases} \dot{X} = A_2 X + B_2 u \\ y = E_2 X + F_2 u \end{cases}. \tag{16}$$

The duty cycle $d(t)$ may now be a time-varying quantity. It is assumed that the natural frequencies of the converter network are much smaller than the switching frequency. This assumption coincides with the small ripple approximation, and is usually satisfied in well-designed converters. It allows the high-frequency switching harmonics to be removed by an averaging process. In addition, the waveforms are linearized about a dc quiescent operating point. The converter waveforms are expressed as quiescent values plus small ac variations as follows [46]:

$$\begin{aligned} x(t) &= X + \hat{x}(t) \\ u(t) &= U + \hat{u}(t) \\ y(t) &= Y + \hat{y}(t) \\ d(t) &= D + \hat{d}(t). \end{aligned} \tag{17}$$

The small-signal ac model is then obtained as

$$\begin{cases} \frac{d\hat{x}(t)}{dt} = A\hat{x}(t) + B\hat{u}(t) + M\hat{d}(t) \\ \hat{y}(t) = E\hat{x}(t) + F\hat{u}(t) + H\hat{d}(t) \end{cases} \tag{18}$$

where

$$\begin{aligned} A &= DA_1 + (1-D)A_2 \\ B &= DB_1 + (1-D)B_2 \\ E &= DE_1 + (1-D)E_2 \\ F &= DF_1 + (1-D)F_2 \end{aligned} \tag{19}$$

and

$$\begin{aligned} M &= (A_1 - A_2)X + (B_1 - B_2)U \\ H &= (E_1 - E_2)X + (F_1 - F_2)U. \end{aligned} \tag{20}$$

Using (9)–(20) yields the following matrices

$$A = \begin{bmatrix} -\frac{R}{L} & -\frac{1}{L} & \frac{D}{L} \\ \frac{1}{C_2} & -\frac{1}{R_o C_2} & 0 \\ -\frac{D}{C_1} & 0 & 0 \end{bmatrix}, B = \begin{bmatrix} 0 \\ 0 \\ \frac{1}{C_1} \end{bmatrix}, M = \begin{bmatrix} \frac{V_{\rm in}}{L} \\ 0 \\ -\frac{I_L}{C_1} \end{bmatrix}$$
$$E = [0\ 0\ 1], F = 0, H = 0.$$

The state-space averaged model that describes the quiescent converter waveforms is

$$\begin{cases} 0 = AX + BU \\ Y = EX + FU \end{cases} \tag{21}$$

The steady-state solution of the converter is, therefore

$$G_{\rm in} = \frac{V_{\rm in}}{I_{\rm in}} = E(-A)^{-1}B + F. \tag{22}$$

This equation yields

$$G_{\rm in} = \frac{R + R_o}{D^2}. \tag{23}$$

If the inductor resistance is negligible, the steady-state solution is equivalent to

$$\frac{V_{\rm in}}{I_{\rm in}} = \frac{R_o}{D^2}. \tag{24}$$

Equation (24) represents the dc equivalent input impedance of the buck converter [12], [13].

Referring back to the small signal model (18), the control to PV voltage transfer function can be obtained as

$$G_c(s) = \frac{\hat{v}_{\rm in}(s)}{\hat{d}(s)} = E(sI - A)^{-1}M \tag{25}$$

which can be simplified in the following form:

$$G_c(s) = -\left(\frac{b_2 s^2 + b_1 s + b_0}{s^3 + a_2 s^2 + a_1 s + a_0}\right) \tag{26}$$

where

$$b_0 = \frac{I_L}{LC_1C_2} + \frac{(DV_{\text{in}} + I_L R)}{R_o LC_1C_2},$$
$$b_1 = \frac{1}{C_1}\left(\frac{DV_{\text{in}}}{L} + \frac{I_L R}{L} + \frac{I_L}{R_o C_2}\right), b_2 = \frac{I_L}{C_1}$$
$$a_0 = \frac{D^2}{LR_oC_1C_2}, a_1 = \frac{R}{LR_oC_2} + \frac{1}{LC_2} + \frac{D^2}{LC_1},$$
$$a_2 = \frac{1}{R_oC_2} + \frac{R}{L}.$$

This equation describes how small ac variations in the duty cycle excite variations in the PV panel voltage.

III. Proposed Dual-MPPT System

The proposed DSP-based standalone photovoltaic system consists of two main subsystems; an astronomical two-axis tracker combined with an MPPT-based buck converter. Both subsystems are controlled through two TMS320F28335 eZdsp boards. Fig. 8 shows the overall system architecture.

The TMS320F28335 DSP from Texas Instruments has a high performance CMOS technology with 150-MHz clock frequency, 3.3-V I/O design and 5-V dc power supply. The DSP includes also a 32-bit CPU with an IEEE-754 single-precision floating point unit for fast interrupt response, efficient programming in C/C++ and Assembly, and a unified memory programming model. The DSP contains six channels for direct memory access (DMA), which is used for ADC, PWM, McBSP (multichannel buffered serial port), XINTF (external interface), and SARAM (single-access RAM). In addition, the DSP supplies a great deal of operations compared to its small size. The DSP provides up to 18 ePWM (enhanced PWM) outputs, 6 HRPWM (high-resolution PWM) outputs, 6 eCAP (enhanced capture) inputs, 2 quadrature encoder interfaces, three 32-bit CPU timers, 2 CAN (controller area network) modules, and one 16 channel 12-bit ADC with a conversion time of 80 ns. The F28335 DSP has also a 512-KB flash and a 68-KB RAM.

A. FLC-Based MPPT

The proposed MPPT controller builds upon the simplicity of the P&O technique but eliminates the resulting steady state oscillations by adaptively modifying the reference voltage perturbation step-size C using a fuzzy logic controller.

The PV panel power is computed from the panel voltage and current and then the absolute value of the power slope $S_a = |dP_{pv}/dV_{pv}|$ is computed and fed to the FLC along with the old step value C_{old}. The fuzzy logic algorithm then outputs the change in the step value ΔC which is added to the old step and then given to the P&O to adjust the reference voltage.

Each input consists of three normalized membership functions: Small, Medium, and Large, whereas the output consists of five normalized membership functions: Negative Big (NB), Negative Small (NS), Zero (Z), Positive Small (PS), and Positive Big (PB).

Depending on the value of the absolute power slope the panel PV curve is divided into three regions, as shown in Fig. 7. Given the old reference voltage perturbation step (C_{old}) the controller will determine the change to the new step in order to reach the MPP. If the operating point was at P_1, where the absolute slope

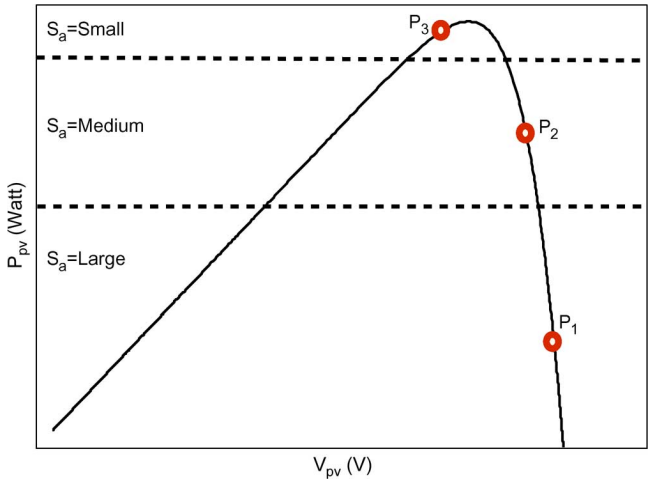

Fig. 7. FLC-based P&O PV curve illustration.

TABLE II
FLC Rules

S = dP/dV \ C_{old}	Small	Medium	Large
Small	ZO	NS	NB
Medium	PS	ZO	NS
Large	PB	PS	ZO

S_a is Large (which means that the operating point is far from the MPP), and if the old step C_{old} is Small, then the change in step size ΔC has to be PB in order to rapidly reach the MPP. Whereas if the old step is also Large the change in step has to be Small in order to avoid exceeding the MPP in the opposite direction leading to oscillations. As a result the FLC consists of the nine rules shown in Table II.

As shown in Fig. 8, the fuzzification block converts the real number "crisp" inputs to fuzzy sets, and then the inference mechanism uses the fuzzy rules of the rule-base to produce the implied fuzzy sets or the fuzzy premises and conclusions. The membership functions (MF) have a triangular waveform as given below for the case of the normalized Medium MF

$$\mu^{\text{Medium}}(u) = \begin{cases} \max\left\{0, 1 + \frac{u-0.5}{0.5}\right\}, & \text{if } u \le 0.5 \\ \max\left\{0, 1 + \frac{0.5-u}{0.5}\right\}, & \text{otherwise} \end{cases}. \quad (27)$$

Similar equations are also defined for the rest of the input and output membership functions.

The premise and conclusion functions are derived using the rule-base given in Table II. Below is as an example for the first rule.

— Rule 1: **If** S_a is Large **and** C_{old} is Small **Then** ΔC is Positive Big

$$\text{Premise}: \mu_{premise(1)} = \min\left(\mu_{\text{Large}}(S_a), \mu_{\text{Small}}(C_{\text{old}})\right) \quad (28)$$
$$Conclusion: \mu(\Delta C)_{(1)} = \min\left\{\mu_{PB}(\Delta C), \mu_{premise(1)}\right\}. \quad (29)$$

The last step in the FLC process is the defuzzification block, which converts the fuzzy conclusions into the crisp real number

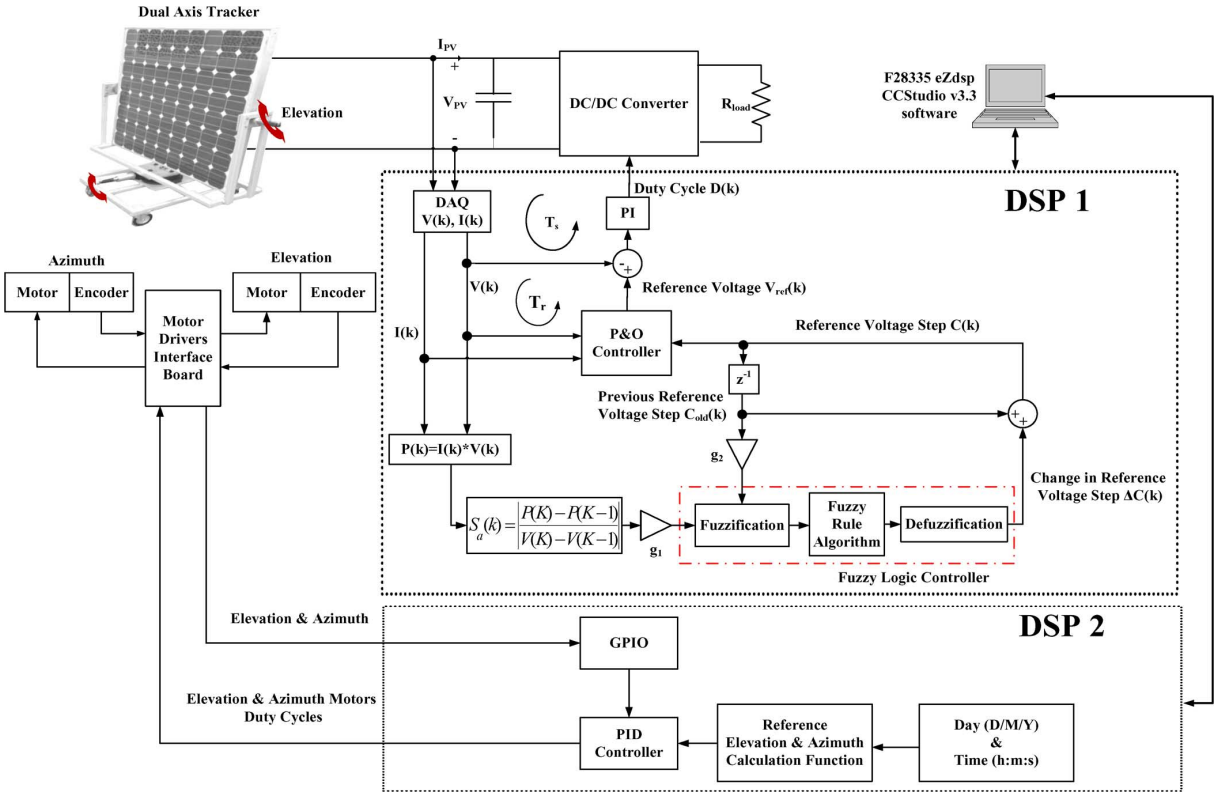

Fig. 8. The proposed DSP-based standalone solar energy system.

outputs. The center of gravity (COG) defuzzification method [47] is used in this work.

Substituting with the premises values, the crisp output function can be expressed as shown in (30) at the bottom of the page, where

$$\int \mu(\Delta C)_{(i)} = \mu_{premise(i)} - \frac{\left(\mu_{premise(i)}\right)^2}{2}, for\ i = 1:9. \tag{31}$$

B. P&O Voltage Control Loop

The inner voltage control loop is implemented using a discrete PI controller

$$e(k) = \hat{v}_{\text{ref}}(k) - \hat{v}_{\text{in}}(k) \tag{32}$$

$$I(k) = I(k-1) + T_s e(k) \tag{33}$$

$$\hat{d}(k) = -\left[K_p e(k) + K_i I(k)\right]. \tag{34}$$

The PI controller gains are designed through the discrete root locus method using the small signal model transfer function $G_c(s)$, as shown in Fig. 9. The discrete transfer function with a zero-order hold is obtained using the Buck converter parameters given in Table III and the nominal parameters under MPP (V_{in}, I_{in}, D). These parameters were obtained by a combination of simulation and measurement with the standard P&O algorithm.

The discrete transfer function shows one zero at -2.67, two complex conjugate poles at $z = -0.5370 \pm j0.0976$, and a pole-zero cancellation at $z = 0$

$$G_c(z) = (1 - z^{-1}) \times Z\left(\frac{G_c(s)}{s}\right) = \frac{-16.35(z + 2.67)(z + 2 \times 10^{-7})}{z(z^2 + 1.074z + 0.2978)}. \tag{35}$$

$$\begin{aligned}\Delta C^{crisp} = {} & \frac{(-1)\int \mu(\Delta C)_{(9)} + (-0.5)\int \mu(\Delta C)_{(8)} + (0)\int \mu(\Delta C)_{(7)}}{\sum_{i=1}^{9}\int \mu_{(i)}(\Delta C)} \\ & + \frac{(-0.5)\int \mu(\Delta C)_{(6)} + (0)\int \mu(\Delta C)_{(5)} + (0.5)\int \mu(\Delta C)_{(4)}}{\sum_{i=1}^{9}\int \mu_{(i)}(\Delta C)} \\ & + \frac{(0)\int \mu(\Delta C)_{(3)} + (0.5)\int \mu(\Delta C)_{(2)} + (1)\int \mu(\Delta C)_{(1)}}{\sum_{i=1}^{9}\int \mu(\Delta C)_{(i)}}\end{aligned} \tag{30}$$

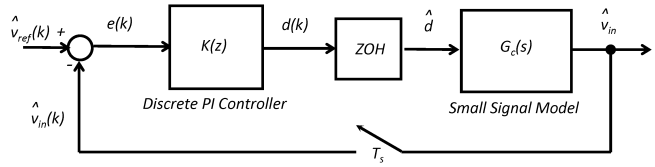

Fig. 9. Discrete PI controller design for the inner voltage control loop.

TABLE III
BUCK CONVERTER PARAMETERS

C_1	C_2	L	R	R_O	V_{in}	I_{in}	D
470 µF	330 µF	0.33 H	0.074 Ω	1.4 Ω	11.64 V	7.8 A	0.92

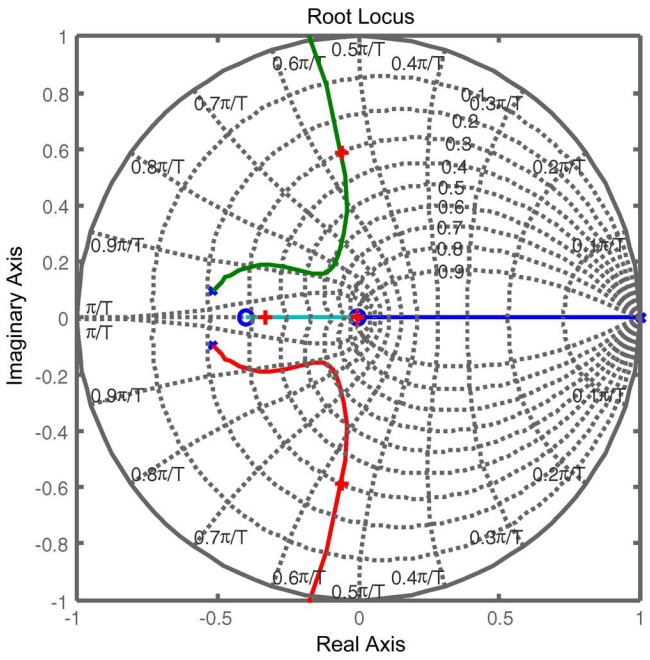

Fig. 10. Discrete root locus for reference voltage control with a PI controller.

Fig. 10 shows the discrete root locus designed for a sampling time $T_s = 0.3\ s$ to have a closed-loop system with an underdamped step response and a settling time t_s less than 5 s. The step response of the reference voltage control system with the obtained PI controller gains $K_p = 0.01$ and $K_i = 0.05$ is shown in Fig. 11. The validation of these gains through outdoor experiments is given in Section VI for the prototype PV system.

IV. STABILITY ANALYSIS

The optimization of the Fuzzy-MPPT algorithm is carried out by selecting the optimum choice of three main parameters characterizing the dynamic behavior of the whole system composed by the buck converter, PV array, and MPPT controller. These parameters are the PI controller gains (K_p, K_i) of the inner voltage control loop, the sampling interval T_r of the reference voltage, and the amplitude of the reference voltage perturbation C. While the amplitude of the reference voltage perturbation is optimized by the Fuzzy logic subsystem, as illustrated in Fig. 8, the stability of the whole system can be achieved by appropriate design of the PI controller and by proper selection of the sampling interval T_r.

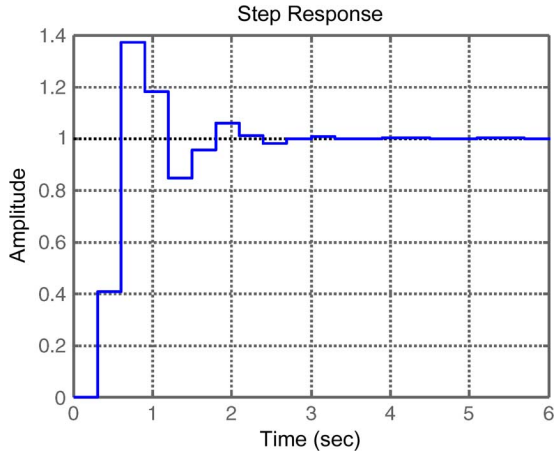

Fig. 11. Step response of the reference voltage control loop with a discrete PI controller ($K_p = 0.01, K_i = 0.05, T_s = 0.3$ s).

The stability of the inner voltage control loop can be analyzed using the Lyapunov stability method. A positive definite function V(t) is defined as

$$V(t) = \frac{1}{2}e^2(t) \tag{36}$$

where $e = V_{\text{ref}} - V_{\text{in}}$ and $de/dt = -(dV_{\text{in}}/dt)$

For step input reference, the derivative of $V(t)$ with respect to time is

$$\frac{dV(t)}{dt} = e(t)\frac{d(V_{\text{ref}} - V_{\text{in}})}{dt} \tag{37}$$

$$\frac{dV(t)}{dt} = -e(t)\frac{dV_{\text{in}}}{dt}. \tag{38}$$

Taking the derivative of the buck converter input V_{in} with respect to time gives

$$\frac{dV_{\text{in}}}{dt} = \frac{dV_{\text{in}}}{dD}\frac{dD}{dt} \tag{39}$$

Defining a PI controller as $u = K_p e + K_i \int e\ dt$ and the duty cycle $D = (1 - u) = 1 - K_p e - K_i \int e\ dt$.

The derivative of the control signal with respect to time is

$$\frac{dD}{dt} = -K_p\frac{de}{dt} - K_i e \tag{40}$$

$$\frac{dD}{dt} = K_p\frac{dV_{\text{in}}}{dt} - K_i e. \tag{41}$$

Substitute dD/dt in (39)

$$\frac{dV_{\text{in}}}{dt} = \left(K_p\frac{dV_{\text{in}}}{dt} - K_i e\right)\frac{dV_{\text{in}}}{dD}. \tag{42}$$

Hence

$$\frac{dV_{\text{in}}}{dt}\left(1 - K_p\frac{dV_{\text{in}}}{dD}\right) = -K_i e\frac{dV_{\text{in}}}{dD} \tag{43}$$

$$\frac{dV_{\text{in}}}{dt} = \frac{-K_i e\frac{dV_{\text{in}}}{dD}}{\left(1 - K_p\frac{dV_{\text{in}}}{dD}\right)}. \tag{44}$$

As a result

$$\frac{dV(t)}{dt} = \frac{K_i e^2 \frac{dV_{\rm in}}{dD}}{\left(1 - K_p \frac{dV_{\rm in}}{dD}\right)}. \tag{45}$$

Therefore, in order to prove the system stability, $dV(t)/dt$ can be made negative if $K_p > 0$, $K_i > 0$ and the system sensitivity function $(dV_{\rm in}/dD) < 0$.

From the buck converter model equation (24), we have $V_{\rm in} = I_{\rm in}R_{\rm in} = I_{\rm in}(R_o/D^2)$. Using this equation in connection with the PV panel IV characteristics, we can observe the following two operating modes.

— If the duty cycle D increases, then (R_o/D^2) decreases and $I_{\rm in}$ will increase. As a result, $V_{\rm in}$ will decrease.

— If the duty cycle D decreases, then (R_o/D^2) increases and $I_{\rm in}$ will decrease. As a result, $V_{\rm in}$ will increase.

This shows that the rate of change in voltage is always opposite to the rate of change in duty cycle. This can be expressed in mathematical form as

$$\frac{dV_{\rm in}}{dt} = -K sign\left(\frac{dD}{dt}\right) \tag{46}$$

where K is a positive gain factor.

Multiplying both sides of (46) by dD/dt gives

$$\left(\frac{dV_{\rm in}}{dD}\frac{dD}{dt}\right)\frac{dD}{dt} = -K\frac{dD}{dt}sign\left(\frac{dD}{dt}\right) \tag{47}$$

$$\frac{dV_{\rm in}}{dD}\left(\frac{dD}{dt}\right)^2 = -K\frac{dD}{dt}sign\left(\frac{dD}{dt}\right). \tag{48}$$

Since $(dD/dt)sign(dD/dt) > 0$ then $dV_{\rm in}/dD$ is always negative. As a result $(dV(t)/dt) < 0$ and the inner voltage control loop is stable.

Next, the stability of the Fuzzy-MPPT can be achieved by proper selection of the reference voltage sampling interval T_r as follows. The sampling interval should be set higher than a proper threshold in order to avoid instability of the MPPT algorithm and to reduce the number of oscillations around the MPP in steady state. If the array voltage and current are sampled too fast, the algorithm may be subjected to possible mistakes caused by the transient behavior of the whole system, thus missing, even if temporarily, the current MPP of the PV panel, which is assumed to be in steady-state operation. As a result, the energy efficiency decays as the algorithm can be confused and the operating point can become unstable, entering disordered and/or chaotic behaviors [48].

To avoid this potential problem, it must be ensured that, after each reference voltage perturbation, the system reaches steady-state before the next measurement of array voltage and current is done.

Assume that the inner voltage loop is designed to behave like a second order dominant system with a desired maximum overshoot M_p and 2% settling time t_s. Then, $\hat{v}_{\rm in}$ will keep within the 2% range of the reference voltage if the sampling interval T_r is higher than t_s ($T_r \gg t_s$). As shown in Section III-B, the PI controller can be designed using the discrete root locus method to achieve this condition and guaranty the P&O stability.

Finally, the stability of the Fuzzy-MPPT is studied by analyzing the recursive equations of the overall Fuzzy-MPPT algorithm

$$V_{\rm ref}(k) = V_{\rm ref}(k-1) + sign\,(S(k)) \times C(k) \tag{49}$$

$$C(k) = C(k-1) + f\,(S_a(k), C(k-1)) \tag{50}$$

where

$$S(k) = \frac{\Delta P(k)}{\Delta V(k)} = \frac{P(k) - P(k-1)}{V(k) - V(k-1)} \tag{51}$$

$$S_a(k) = |S(k)| = \left|\frac{\Delta P(k)}{\Delta V(k)}\right|. \tag{52}$$

In steady state

$$\begin{aligned} V_{\rm ref}(k) &= V_{\rm ref}(k-1) = V_{{\rm ref},ss} \\ C(k) &= C(k-1) = C_{ss} = 0 \\ S(k) &= S(k-1) = S_{ss} = 0. \end{aligned} \tag{53}$$

As a result, in order to prove the convergence of the Fuzzy-MPPT algorithm, the following condition should be satisfied: $\lim_{S_a, C\to 0} f(S_a(k), C(k-1)) = 0$.

This limit can be found through the crisp output function given by

$$\lim_{S_a, C\to 0} f\,(S_a(k), C(k-1)) = \lim_{S_a, C_{\rm old}\to 0}(\Delta C^{\rm crisp}). \tag{54}$$

Finding the limits of the different premises, it can be shown that

$$\lim_{S_a, C_{\rm old}\to 0}\left[\mu_{premise(i)}\right] = 0.\ For\ i = 1:9\ and\ i \neq 7 \tag{55}$$

$$\lim_{S_a, C_{\rm old}\to 0}\left[\mu_{premise(7)}\right] = 1 \tag{56}$$

and

$$\lim_{S_a, C_{\rm old}\to 0}\sum_{i=1}^{9}\int \mu(\Delta C)_{(i)} = 0.5 \tag{57}$$

where

$$\mu_{premise(7)} = \min\left(\mu_{\rm Small}(S_a), \mu_{\rm Small}(C_{\rm old})\right). \tag{58}$$

Therefore

$$\lim_{S_a, C_{\rm old}\to 0} \Delta C^{\rm crisp} = 0. \tag{59}$$

This proves that if the system reaches MPP where $V_{\rm ref}(k)$ is equal to $V_{{\rm ref},ss}$, the FLC output will be zero and the system will continue operating at the same MPP corresponding to the given temperature and insolation conditions.

V. Simulation Results

In order to verify the proposed controller operation, the FLC-based P&O MPPT was integrated into the Simulink PV panel model derived in Section II. Through simulation the proposed technique is compared to the conventional P&O MPPT with two

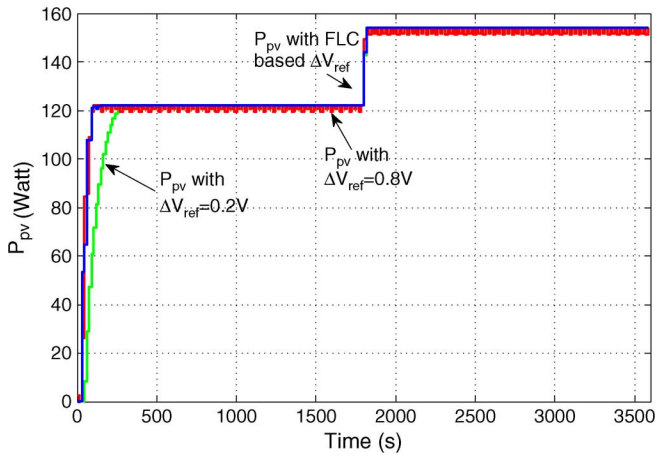

Fig. 12. P&O algorithms power curves comparison. Simulation results with sun insolation step changes at $t = 0$ s from 0 to 800 W/m^{2}and at $t = 1800$ s from 800 to 1000 W/m^2 and $T = 25$ °C.

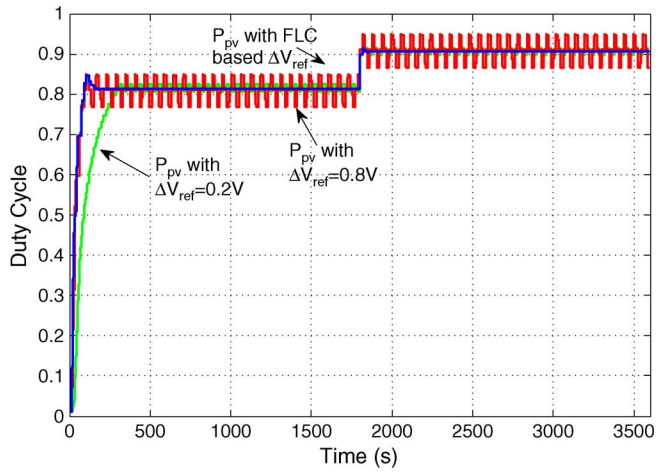

Fig. 13. Duty cycle curves comparison. Simulation results with sun insolation step changes at $t = 0$ s from 0 to 800 W/m^2 and at $t = 1800$ s from 800 to 1000 W/m^2 and $T = 25$ °C.

different duty cycle steps under varying insolation conditions. The inner-voltage control loop sampling time T_s was set to 0.3 s, while the P&O sampling time T_r was set to be 15 s in order to give the PV voltage enough time to reach the reference value before the next step perturbation.

Fig. 12 shows the PV panel power curves for three controllers: P&O with voltage step 0.8 V, P&O with voltage step 0.2 V, and Fuzzy-based P&O. The results clearly shows that the proposed Fuzzy-based P&O has a better performance compared to the conventional P&O (faster settling time and less steady-state oscillations) resulting in higher energy.

Fig. 13 further illustrates the superiority of the proposed technique as it shows the overall controller output (duty cycle) produced by the three controllers. The results clearly illustrates that the FLC-based P&O reaches faster to the optimal duty cycle with less oscillations compared to the conventional P&O. The FLC-based P&O has also a faster response to the change in insolation condition.

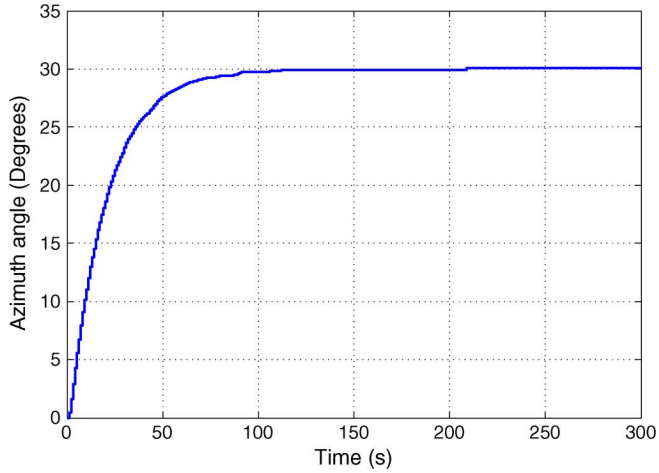

Fig. 14. Experimental position step response (30°) for the azimuth axis.

VI. Experimental Results

The 150-Watt PV system was implemented as shown in Fig. 8. The control algorithms are developed on two separate DSPs. The first DSP is solely dedicated to the solar tracker while the second DSP is for the FLC-based MPPT.

The control code is developed by the operator on a laptop using Code Composer Studio and then downloaded on the DSPs for real time operation. Code Composer Studio is an integrated environment used to support the TMS320F28335 DSP software development. The programming environment is a practical and user friendly tool, which includes an editor, a code generation tool, a debugger, a project manager, and a profiler. Code Composer Studio also provides probe points, real-time analysis, and visualization tools.

The MPPT algorithm is divided in four main program components: Data acquisition of the PV panel voltage and current (DAQ), PI controller for the PV voltage loop, P&O controller and Fuzzy Logic controller (FLC). The control algorithm is implemented as a timer-interrupt driven routine with a sampling time $T_s = 0.3$ s. The P&O and FLC are executed only every sampling time $T_r = 50T_s = 15$ s. The execution time of all four routines is within the sampling time 0.3 s.

The two-axis solar tracker is implemented using a closed loop digital position control system with a discrete PID controller for each axis (Fig. 5). The PID gains were tuned to achieve an overdamped response with zero steady-state error and a 2% settling time of around 87 s. Fig. 14 shows the response of the azimuth axis to a step reference with amplitude 30°.

The performance of the inner MPPT voltage control loop is verified using step changes to the voltage reference. Fig. 15 shows the response of the system to large and small voltage steps.

For the system under consideration, the same PI controller gains designed in Section II-B $K_p = 0.01$, $K_i = 0.05$ are used and yield a settling time $t_s = 4.8$ s as desired. A sampling interval $T_r = 15$ s is used in order to guaranty that the MPPT is not affected by mistakes caused by intrinsic transient oscillations of the PV system.

Next, in order to analyze the dual-MPPT system operation, three tests were performed.

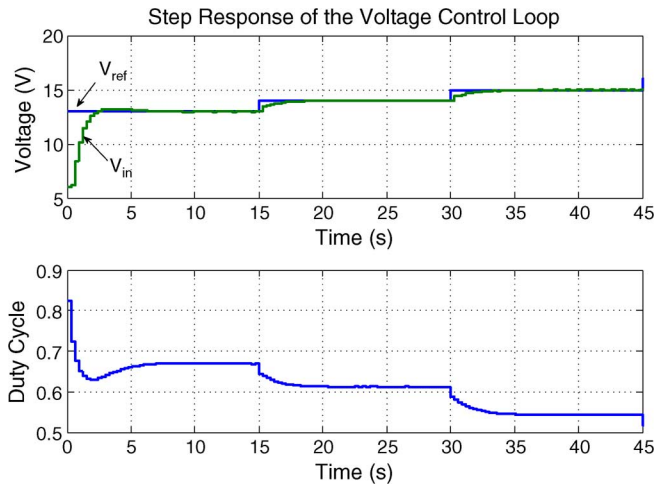

Fig. 15. Inner voltage control loop step response.

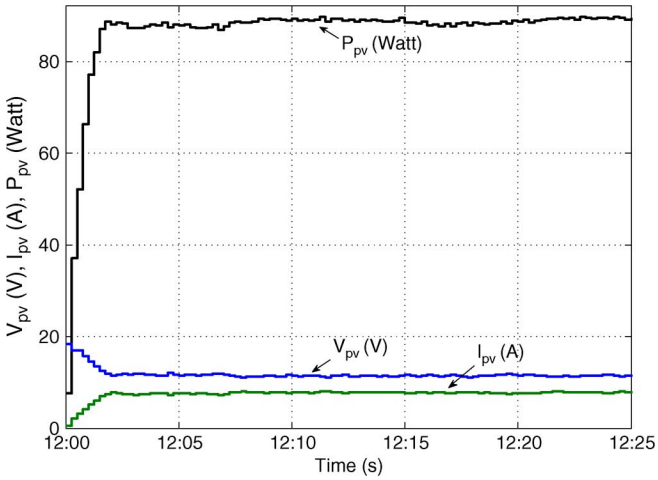

Fig. 16. FLC-based P&O experimental results (Nov. 21, 2011, 12:00–12:25 pm).

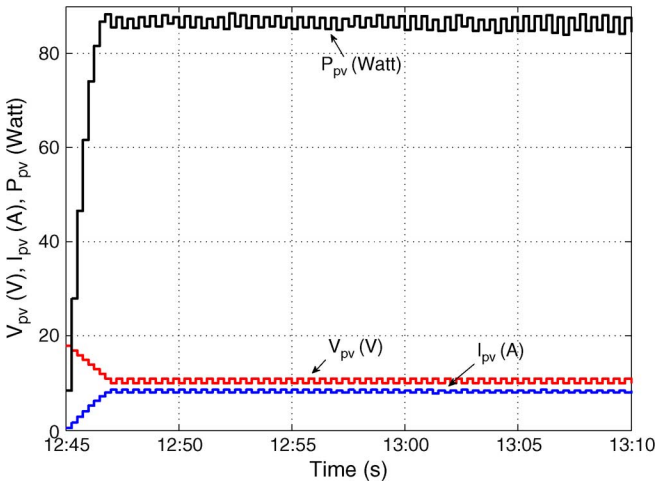

Fig. 17. P&O experimental results with $\Delta V_{\rm ref} = 0.8$ V (Nov. 21, 2011, 12:45–13:10 pm).

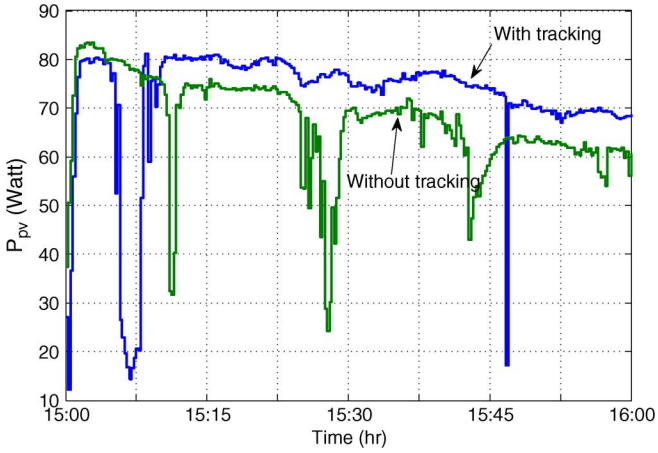

Fig. 18. Experimental results for FLC-based P&O with and without sun tracking (with tracking: Nov. 24, 2011, 3–4 pm, without tracking: Nov. 25, 2011, 3–4 pm).

— Test 1: Fixed panel with conventional P&O MPPT.
— Test 2: Fixed panel with FLC-based P&O MPPT.
— Test 3: Dual axis tracking of the panel with FLC-based P&O MPPT.

Tests 1 and 2 compare between the proposed technique and the conventional P&O. In both tests the PV panel was fixed facing south with an elevation of 52°. The experimental results of the proposed FLC-MPPT technique are shown in Fig. 16. The results show that the maximum power is reached within a short time (five samples) and the oscillations around the MPP are minimal. On the other hand, with the conventional P&O and a fixed step size ($C = 0.8$), the response is slower as it reaches the MPP within six samples and keep oscillating around it as shown in Fig. 17. These results highlight clearly the features of the proposed fuzzy-based MPPT which improves the efficiency of the system by yielding higher power, while eliminating the steady-state oscillations around the MPP.

Tests 1 and 3 compare the performance between the fixed panel and the dual axis tracking. Test 3 involved applying the physical tracking algorithm on the panel with the FLC-based P&O. The tests were carried out in two consecutive days for 1 h in the afternoon with similar cloudy weather conditions. As shown in Fig. 18, the tracking yielded higher power and the degradation of the power within the 1 h of testing was lower. Moreover, Fig. 18 shows the response of the MPPT proposed technique to varying weather conditions (clouds shading) as it was able to track the maximum power operating point as soon as the panel was unshaded.

TABLE IV
ENERGY YIELDED IN kWh

Test No.	Test Type	Average Power (kW)	E (kWh)
1	P&O with fixed ΔV_{ref}=0.8	0.08431	0.03513
2	FLC based P&O	0.08650	0.03604
3.a	FLC based P&O with sun tracking	0.07205	0.07205
3.b	FLC based P&O without sun tracking	0.06700	0.06700

Table IV shows the yielded energy in kWh from the three tests. The energy is calculated using the following equation:

$$E(k) = \sum_{k=1}^{N} (P(k)T_r) = P_{\rm Average} \times (NT_r) \qquad (60)$$

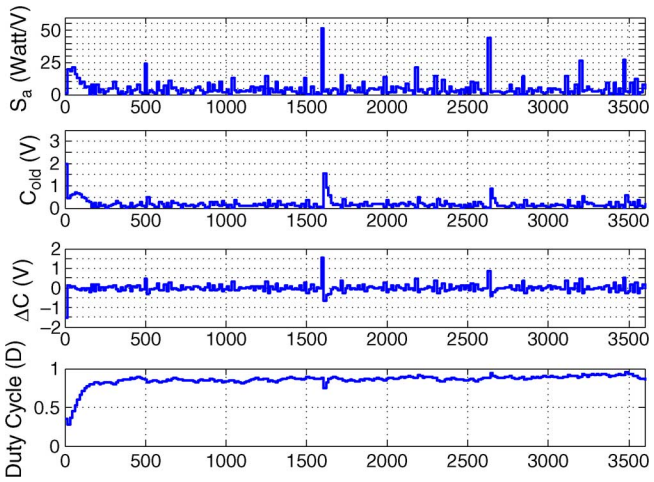

Fig. 19. FLC inputs and output for a clear day with multiple shading disturbances.

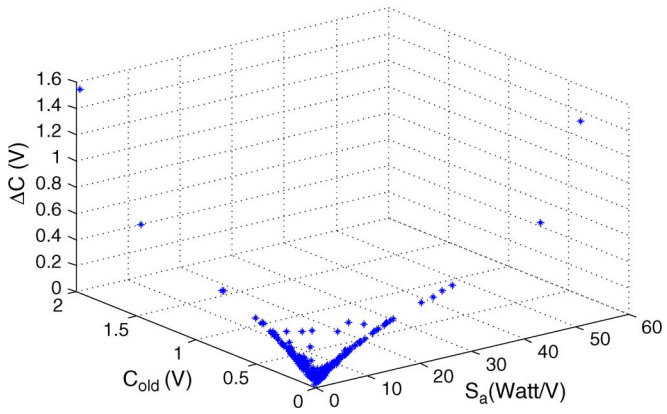

Fig. 20. FLC absolute output as a function of the two inputs.

where (NT_r) is the testing time period. The proposed FLC-based P&O technique yielded an enhancement of 2.53% in energy when the panel is fixed, whereas introducing the sun tracking yielded an enhancement of 7% in energy.

In order to check the stability of the FLC-MPPT algorithm, the system inputs and outputs are plotted for 1 h of testing. As shown in Fig. 19, the duty cycle reaches the MPP and keeps operating around it while the FLC system output converges to zero. Moreover, Fig. 19 shows the ability of the system to act against disturbances as it goes back to the steady state once the disturbances are cleared. Plotting the absolute value of the FLC output as a function of the two FLC inputs in a 3D plot shows that the system output converges to zero in steady state, as shown in Fig. 20.

For the standard P&O controller with a fixed voltage perturbation step, the operating point is continuously perturbed causing the PV array terminal voltage to fluctuate around the MPP voltage even if the solar irradiance and the cell temperature are constants. The step size must also be high enough to allow the perturbation to cause a measurable change in array output power. Noise has considerable effect on the MPPT algorithm performance, especially at low step sizes where the system response to noise is comparable to that of the MPPT perturbations.

For the proposed FLC-based controller, the perturbation step size is adapted online by the FLC-MPPT and the step size is shown to converge to zero as the system reached MPP. In addition, the inclusion of a PI controller in the voltage control loop eliminates the steady state error and makes the system less sensitive to noise. The measurement noise in voltage and current leads to a superposed noise on the measured power. The operating point may be therefore perturbed causing the PV array terminal voltage to fluctuate around the MPP voltage even if the solar irradiance and the cell temperature are constants. The outdoor experimental results obtained with the proposed algorithm show that the system has a good noise rejection and the fluctuations around the MPP are minimal, as shown in Fig. 20.

VII. Conclusion

This paper presents a new digital control scheme for a standalone photovoltaic system using fuzzy-logic and a dual-MPPT controller. The MPPT controller is combined with a dual-axis panel tracking controller to improve the efficiency of the overall system. The proposed control scheme takes the power slope of the PV panel curve and the old voltage perturbation step as its inputs and outputs the change in the new P&O step size. The FLC output is gradually updated in order to avoid exceeding the MPP in the opposite direction leading to oscillations. The controller was implemented on a 150-Watt prototype PV system. Simulation and experimental results show clearly the advantages of the proposed technique compared to the conventional P&O. The proposed technique is able to reduce the steady state oscillations and enhance the operating point convergence speed.

References

[1] G. Spagnuolo, G. Petrone, S. V. Araujo, C. Cecati, E. Friis-Madsen, E. Gubia, D. Hissel, M. Jasinski, W. Knapp, M. Liserre, P. Rodriguez, R. Teodorescu, and P. Zacharias, "Renewable energy operation and conversion schemes," *IEEE Ind. Electron. Mag.*, vol. 4, no. 1, pp. 38–51, Mar. 2010.

[2] P. Fairley, "Fukushima's positive impact [spectral lines]," *IEEE Spectrum*, vol. 48, no. 5, p. 8, May 2011.

[3] B. Bose, "Global warming: Energy, environmental pollution, and the impact of power electronics," *IEEE Ind. Electron.*, vol. 4, no. 1, pp. 6–17, Mar. 2010.

[4] H. Mousazadeh, A. Keyhani, A. Javadi, and H. Mobli, "A review of principle and sun-tracking methods for maximizing solar systems output," *Renewable and Sustainable Energy Reviews*, vol. 13, pp. 1800–1818, 2009.

[5] M. Clifford and D. Eastwood, "Design of a novel passive solar tracker," *Solar Energy*, vol. 77, pp. 269–280, 2004.

[6] R.-J. Wai, W.-H. Wang, and C.-Y. Lin, "High-performance stand-alone photovoltaic generation system," *IEEE Trans. Ind. Electron.*, vol. 55, no. 1, pp. 240–250, Jan. 2008.

[7] C. Chin, A. Babu, and W. McBride, "Design, modeling and testing of a standalone single axis solar tracker using MATLAB/Simulnik," *Renewable Energy*, vol. 36, pp. 3075–3090, 2011.

[8] H. Lu and T. Shih, "Fuzzy system control design with application to solar panel active dual-axis Sun tracker system," in *Proc. SMC'10*, Istanbul, 2010, pp. 1878–1883.

[9] S. Abdallah and O. Badran, "Sun tracking system for productivity enhancement of solar still," *Desalination*, vol. 220, pp. 669–676, 2008.

[10] S. Seme, G. Štumberger, and J. Voršič, "Maximum efficiency trajectories of a two-axis sun tracking system determined considering tracking system consumption," *IEEE Trans. Power Electron.*, vol. 26, no. 4, pp. 1280–1290, Apr. 2011.

[11] A. Al Nabulsi, A. El Nosh, A. Ahli, M. Sulaiman, and R. Dhaouadi, "Efficiency optimization of a 150W PV system using dual axis tracking and MPPT," in *Proc. IEEE ENERGYCON'10*, Bahrain, pp. 400–405.

[12] E. Aranda, J. Galá N, M. Cardona, and J. Rquez, "Measuring the i-v curve of PV generators," *IEEE Ind. Electron. Mag.*, vol. 3, no. 3, pp. 4–14, Sep. 2009.
[13] R. F. Coelho, F. M. Concer, and D. C. Martins, "Analytical and experimental analysis of DC-DC converters in photovoltaic maximum power point tracking applications," in *Proc. IECON'10*, Phoenix, AZ, 2010, pp. 2778–2783.
[14] W. Xiao, W. G. Dunford, P. R. Palmer, and A. Capel, "Regulation of photovoltaic voltage," *IEEE Trans. Ind. Electron.*, vol. 54, no. 3, pp. 1365–1374, Jun. 2007.
[15] G. Petrone, G. Spagnuolo, R. Teodorescu, M. Veerachary, and M. Vitelli, "Reliability issues in photovoltaic power processing systems," *IEEE Trans. Ind. Electron.*, vol. 55, no. 7, pp. 2569–2580, Jul. 2008.
[16] T. Patrick and P. Chapman, "Comparison of photovoltaic array maximum power point tracking techniques," *IEEE Trans. Energy Conv.*, vol. 22, no. 2, pp. 439–449, Jun. 2007.
[17] V. Salas, E. Olias, A. Barrado, and A. Lazaro, "Review of the maximum power point tracking algorithms for stand-alone photovoltaic systems," *Solar Energy Materials Solar Cells*, vol. 90, no. 11, pp. 1555–1578, 2006.
[18] K. K. Tse, M. T. Ho, H. S. Chung, and S. Y. R. Hui, "A comparative study of maximum-power-point trackers for photovoltaic panels using switching-frequency modulation scheme," *IEEE Trans. Ind. Electron.*, vol. 51, no. 2, pp. 410–418, Apr. 2004.
[19] E. B. Youssef, P. Stephane, E. Bruno, and A. Corinne, "New P&O MPPT algorithm for FPGA implementation," in *Proc. IECON'10*, Phoenix, AZ, 2010, pp. 2868–2873.
[20] N. Femia, G. Petrone, G. Spagnuolo, and M. Vitelli, "A technique for improving P&O MPPT performances of double-stage grid-connected photovoltaic systems," *IEEE Trans. Ind. Electron.*, vol. 56, no. 11, pp. 4473–4482, Nov. 2009.
[21] R. Kadri, J. Gaubert, and G. Champenois, "An improved maximum power point tracking for photovoltaic grid-connected inverter based on voltage oriented control," *IEEE Trans. Ind. Electron.*, vol. 58, no. 1, pp. 66–75, Jan. 2011.
[22] L. Fangrui, K. Yong, Z. Yu, and D. Shanxu, "Comparison of P&O and hill climbing MPPT methods for grid-connected PV converter," in *Proc. ICIEA'08*, Singapore, Jun. 2008, pp. 804–807.
[23] J. Jiang, T. Huang, Y. Hsiao, and C. Chen, "Maximum power tracking for photovoltaic power systems," *Tamkang J. Sci. Eng.*, vol. 8, no. 2, pp. 147–153, 2005.
[24] N. Femia, D. Granozio, G. Petrone, G. Spagnuolo, and M. Vitelli, "Predictive & adaptive MPPT perturb and observe method," *IEEE Trans. Aerosp. Electron. Syst.*, vol. 43, no. 3, pp. 934–950, Jul. 2007.
[25] K.-H. Chao and C.-J. Li, "An intelligent maximum power point tracking method based on extension theory for PV systems," *Expert Syst. Appl.*, vol. 37, no. 2, pp. 1050–1055, 2010.
[26] R.-J. Wai, W.-H. Wang, and J.-Y. Lin, "Grid-connected photovoltaic generation system with adaptive step-perturbation method and active sun tracking scheme," *IEEE Trans. Ind. Electron.*, pp. 224–228, Nov. 2006.
[27] C. Ahn, J. Choi, and D. Lee, "Adaptive maximum power point tracking algorithm for photovolatic power systems," *IEICE Trans. Commun.*, vol. E93-B, no. 5, pp. 1334–1337, May 2010.
[28] Q. Mai, M. Shan, L. Liu, and J. M. Guerrero, "A novel improved variable step-size incremental-resistance MPPT method for PV systems," *IEEE Trans. Ind. Electron.*, vol. 58, no. 6, pp. 2427–2434, Jun. 2011.
[29] I. Houssamo, F. Locment, and M. Sechilariu, "Maximum power tracking for photovoltaic power system: Development and experimental comparison of two algorithms," *Renewable Energy*, vol. 35, pp. 2381–2387, 2010.
[30] F. Liu, S. Duan, B. Liu, and Y. Kang, "A variable step size INC MPPT method for PV systems," *IEEE Trans. Ind. Electron.*, vol. 55, no. 7, pp. 2622–2628, Jul. 2008.
[31] A. Safari and S. Mekhilef, "Simulation and hardware implementation of incremental conductance MPPT with direct control method using cuk converter," *IEEE Trans. Ind. Electron.*, vol. 58, no. 4, pp. 1154–1161, Apr. 2011.
[32] M. Veerachary, T. Senjyu, and K. Uezato, "Neural-network-based maximum power point tracking of coupled inductor interleaved-boost converter supplied PV system using fuzzy controller," *IEEE Trans. Ind. Electron.*, vol. 50, no. 4, pp. 749–758, Aug. 2003.
[33] C. B. Salah and M. Ouali, "Comparison of fuzzy logic and neural network in maximum power point tracker for PV systems," *Electric Power Syst. Res.*, vol. 81, pp. 43–50, 2011.
[34] A. Mellita and S. Kalogirou, "Artificial intelligence techniques for photovoltaic applications: A review," *Progress in Energy and Combustion Science*, vol. 34, no. 5, pp. 574–632, Oct. 2008.
[35] J. L. Agorreta, L. Reinaldos, R. Gonzalez, M. Borrega, J. Balda, and L. Marroyo, "Fuzzy switching technique applied to PWM boost converter operating in mixed conduction mode for PV systems," *IEEE Trans. Ind. Electron.*, vol. 56, no. 11, pp. 4363–4373, Nov. 2009.
[36] A. Al-Nabulsi, R. Dhaouadi, and H. Rehman, "Single input fuzzy controller (SFLC) based maximum power point tracking," in *Proc. ICSMAO'11*, Kuala lumpor, 2011, pp. 1–5.
[37] T.-F. Wu, C.-H. Chang, and Y.-H. Chen, "A fuzzy-logic-controlled single-stage converter for PV-powered lighting system applications," *IEEE Trans. Ind. Electron.*, vol. 47, no. 2, pp. 287–296, Apr. 2000.
[38] C.-S. Chiu, "T-S fuzzy maximum power point tracking control of solar power generation systems," *IEEE Trans. Energy Conv.*, vol. 25, no. 4, pp. 1123–1131, Dec. 2010.
[39] I.-S. Kim, M.-B. Kim, and M.-J. Youn, "New maximum power point tracker using sliding-mode observer for estimation of solar array current in the grid-connected photovoltaic system," *IEEE Trans. Ind. Electron.*, vol. 53, no. 4, pp. 1027–1035, Aug. 2006.
[40] W. Xiao, M. G. J. Lind, W. G. Dunford, and A. Capel, "Real-time identification of optimal operating points in photovoltaic power systems," *IEEE Trans. Ind. Electron.*, vol. 53, no. 4, pp. 1017–1026, Aug. 2006.
[41] V. V. R. Scarpa, S. Buso, and G. Spiazzi, "Low-complexity MPPT technique exploiting the PV module MPP locus characterization," *IEEE Trans. Ind. Electron.*, vol. 56, no. 5, pp. 1531–1538, May 2009.
[42] M. Kazmierkowski, M. Jasinski, and G. Wrona, "DSP-based control of grid-connected power converters operating under grid distortions," *IEEE Trans. Ind. Informat.*, vol. 7, no. 2, pp. 204–211, May 2011.
[43] A. Malinowski and H. Yu, "Comparison of embedded system design for industrial applications," *IEEE Trans. Ind. Informat.*, vol. 7, no. 2, pp. 244–254, May 2011.
[44] Y. Wu, G. Buttazzo, E. Bini, and A. Cervin, "Parameter selection for real-time controllers in resource-constrained systems," *IEEE Trans. Ind. Informat.*, vol. 6, no. 4, pp. 610–620, 2010.
[45] Y. Chen, C. Yang, and T. Kuo, "Energy-efficient task synchronization for real-time systems," *IEEE Trans. Ind. Informat.*, vol. 6, no. 3, pp. 287–301, Aug. 2010.
[46] R. W. Erickson and D. Maksimović, *Fundamental of Power Electronics*. Norwell, MA: Kluwer, 2001.
[47] K. Passino and S. Yurkovich, *Fuzzy Control*. Reading, MA, USA: Addison-Wesley, 1998.
[48] D. P. Hohm and M. E. Ropp, "Comparative study of maximum power point tracking algorithms using an experimental, programmable, maximum power point tracking test bed," in *Proc. 28th IEEE Photovoltaic Specialists Conf.*, Anchorage, 2000, pp. 1699–1702.

Ahmad Al Nabulsi was born in 1986. He received the B.Sc. degree in electrical engineering and the M.S. degree in mechatronics engineering from the American University of Sharjah, Sharjah, UAE, in 2009 and 2012 respectively.

He worked as a Graduate Teaching Assistant in the College of Engineering, American University of Sharjah, in 2009 and 2010. His research interests include renewable energy, embedded and control systems.

Rached Dhaouadi (M'90–SM'02) received the Ph.D. degree in electrical engineering from the University of Minnesota, Minneapolis, MN, in 1990.

From 1990 to 1994, he worked as a Visiting Researcher with the Hitachi Research Laboratory, Japan, in the design and development of motor drive systems for rolling mills. From 1994 to 2000, he was with the Polytechnic School of Tunisia, University of Tunis. He also held Visiting Scholar positions at Trondheim Institute of Technology, Norway, and at Rice University, USA. He is currently a Professor of Electrical Engineering at the American University of Sharjah, Sharjah, UAE. His research interests are in the areas of motor drives, renewably energy systems, and intelligent motion control systems.